

Revisiting newly Large Magellanic Cloud age gap star clusters

ANDRÉS E. PIATTI^{1,2}

¹*Instituto Interdisciplinario de Ciencias Básicas (ICB), CONICET-UNCUYO, Padre J. Contreras 1300, M5502JMA, Mendoza, Argentina*

²*Consejo Nacional de Investigaciones Científicas y Técnicas (CONICET), Godoy Cruz 2290, C1425FQB, Buenos Aires, Argentina*

ABSTRACT

Recently, a noticeable number of new star clusters was identified in the outskirts of the Large Magellanic Cloud (LMC) populating the so-called star cluster age gap, a space of time (~ 4 -12 Gyr) where the only known star cluster is up-to-date ESO 121-SC 03. We used Survey of the Magellanic Stellar History (SMASH) DR2 data sets, as well as those employed to identify these star cluster candidates, to produce relatively deep color-magnitude diagrams (CMDs) of 17 out of 20 discovered age gap star clusters with the aim of investigating them in detail. Our analysis relies on a thorough CMD cleaning procedure of the field star contamination, which presents variations in its stellar density and astrophysical properties, such as luminosity and effective temperature, around the star cluster fields. We built star cluster CMDs from stars with membership probabilities assigned from the cleaning procedure. These CMDs and their respective spatial distribution maps favor the existence of LMC star field density fluctuations rather than age gap star clusters, although a definitive assessment on them will be possible from further deeper photometry.

Keywords: methods:observational – technique:photometric – galaxies:individual:LMC – galaxies:star cluster:general

1. INTRODUCTION

The absence of star clusters with ages between ~ 3 and 10 Gyr in the Large Magellanic Cloud (LMC) - the sole exception is ESO 121-SC 03 (Mateo et al. 1986) - was noticed by Olszewski et al. (1991). They also found that the age gap correlates with a cluster metallicity gap, in the sense that star clusters younger than 3 Gyr are much more metal-rich than the ancient LMC globular clusters. The LMC age gap spans most of the galaxy lifetime, thus making difficult to reconstruct its chemical enrichment from cluster ages and metallicities. Although different observational campaigns have searched for unknown old star clusters, they have confirmed previous indications that star clusters were not formed during the age gap (e.g., Da Costa 1991; Geisler et al. 1997).

The upper age limit of the LMC age gap is given by the youngest ages of the 15 LMC globular clusters (~ 12 Gyr, Piatti & Mackey 2018; Piatti et al. 2018b). The lower age limit, however, has been changed as more intermediate-age stars clusters were studied in detail.

For instance, Sarajedini (1998) found that NGC 2121, 2155 and SL 663 are ~ 4 Gyr old star clusters, while Rich et al. (2001) re-estimated their ages to be 0.8 Gyr younger (see, also, Piatti et al. 2002). Age estimates of poorly studied or unstudied star clusters were derived during the last decade, and the oldest ones turned out to be ~ 2.5 -3.0 Gyr old (see, e.g. Piatti et al. 2009; Piatti 2011a; Piatti & Geisler 2013). From the above results, we use here a conservative definition of age gap star clusters as those with ages between 4 and 12 Gyr.

The LMC star cluster age distribution was modeled by Bekki et al. (2004), who proposed that the LMC was formed at a distance from the Milky Way that did not allow its tidal forces to trigger star cluster formation efficiently. The star cluster formation resumed in the LMC at its first encounter with the Small Magellanic Cloud ~ 2 -3 Gyr ago. Such a star cluster formation history was not that of the Small Magellanic Cloud, which would have been formed as a lower mass galaxy closer to the Milky Way, and thus more continuously influenced by its gravitational field. Nevertheless, both Magellanic Clouds have had a series of close interactions between them and their first passage around the Milky Way, that explain their abrupt observed chemical enrichment his-

tory and increase of the star cluster formation rates (Piatti 2011a,b; Piatti & Geisler 2013; Kallivayalil et al. 2013; Lucchini et al. 2020).

Recently, Gatto et al. (2020) performed a search for unidentified star clusters in LMC outermost regions and detected 20 star cluster candidates with estimated ages $\gtrsim 4$ Gyr. They used the YMCA (Yes, Magellanic Clouds Again) and STEP (The SMC in Time: Evolution of a Prototype interacting late-type dwarf galaxy, Ripepi et al. 2014) surveys carried out with the VLT Survey Telescope (VST) at ESO. Because the discovery of only one LMC age gap star cluster would be worth by itself, this astonishing large number of new age gap star cluster candidates caught our attention. The authors mentioned that these candidates come from surveying previously unexplored regions in the LMC periphery and from their deep photometry. While the outermost LMC regions have started to be targeted relatively recently with the aim of looking for new star clusters (see Table 1 in Maia et al. 2019), the depth of the photometric campaigns could even improve (see, e.g., Sarajedini 1998; Rich et al. 2001). In this work, we make use of the same data sets employed by Gatto et al. (2020) and publicly available Survey of the Magellanic Stellar History (SMASH) DR2 data sets (Nidever et al. 2021) to further confirm the ages of the new star cluster candidates, so to reinforce their discoveries. In Section 2, we present the data used in this work, while in Section 3 we describe the analysis carried out in order to unveil the fiducial star cluster features in the color-magnitude diagram (CMD). Finally, in Section 4 we discuss the present results and summarize the main conclusions.

2. THE DATA

We use the portal of the Astro Data Lab¹, which is part of the Community Science and Data Center of NSF’s National Optical Infrared Astronomy Research Laboratory, to retrieve R.A and Dec. coordinates, PSF g, i magnitudes and their respective errors, interstellar reddening $E(B - V)$ and χ and SHARPNESS parameters of stellar sources located inside a radius of $6'$ from the star clusters’ centers listed by Gatto et al. (2020). The retrieved data sets consist of sources with $0.2 \leq \text{SHARPNESS} \leq 1.0$ and $\chi^2 < 0.5$, so bad pixels, cosmic rays, galaxies, and unrecognized double stars were excluded. Gatto et al. (2020) discovered 85 star cluster candidates. In this work we analyze 17 out of 20 objects with estimated ages ≥ 4 Gyr ($\log(\text{age} / \text{yr}) \geq 9.6$). STEP-0004, YMCA-0031, and YMCA-0033 are age gap star cluster candidates, but they fall outside the areal coverage of

SMASH DR2. Figure 1 illustrates a typical star cluster field, where the variation of the interstellar reddening is shown with color-coded symbols.

The radii of the studied star cluster candidates are relatively small, from $0.2'$ up to $0.55'$, with an average of $0.35'$ (see Table B1 in Gatto et al. 2020). Because we downloaded information for circular areas much larger than the star cluster fields, we thoroughly monitored the contamination of field stars in the star clusters’ CMDs. Indeed, we selected for each star cluster field, represented by a circle centered on the star cluster with a radius 3 times that of the star cluster, 6 adjacent reference star field regions of equal star cluster field area distributed around the cluster region, as depicted in Fig. 1. We based our analysis on dereddened CMDs, so we first corrected by interstellar extinction the g and i magnitudes using the $E(B - V)$ values provided by SMASH and the $A_\lambda/E(B - V)$ ratios, for $\lambda = g, i$, given by Abbott et al. (2018). The retrieved SMASH $E(B - V)$ value for each star (see color bar in Fig. 1) corresponds to the median $E(B - V)$ around it obtained by using the Schlegel et al. (1998)’s reddening map (see also Choi et al. 2018; Nidever et al. 2021).

As for the data sets used by Gatto et al. (2020), they were kindly provided by V. Ripepi. We note that the g, i bands of the STEP/YMCA surveys are not the same used by SMASH (see figure 1 in Ripepi et al. 2014). Therefore, $g - i$ color ranges are not straightforwardly comparable, nor their CMDs. Both, STEP/YMCA and SMASH data sets are then independent sources. Nidever et al. (2017) presented in their Table 4 the SMASH average photometric transformation equations. By adding in quadrature zero-point, extinction and color term errors, we computed an accuracy $\lesssim 0.02$ mag in gi . They showed that these calibration errors imply a SMASH photometry precision of ~ 0.5 - 0.7% in gi . Such a precision implies in turn an uncertainty of ~ 0.11 - 0.14 mag in gi , for a star at the main sequence turnoff of a ~ 4 Gyr old LMC star cluster ($g_0 \gtrsim 22.0$ mag). Gatto et al. (2020) obtained an average photometry accuracy of 0.02 - 0.03 mag in g and i , respectively, which is comparable to that of SMASH. We note that the zero point and color terms errors obtained by Ripepi et al. (2014, see their Table 8), on which Gatto et al. (2020)’s photometry relies, are of the same order than those of SMASH.

3. DATA ANALYSIS

The contamination of field stars plays an important role when dealing with star cluster CMDs, because it is not straightforward to consider a star as a cluster member only on the basis of its position in that CMD. Sometimes, additional information like proper motions,

¹ <https://datalab.noao.edu/smash/smash.php>

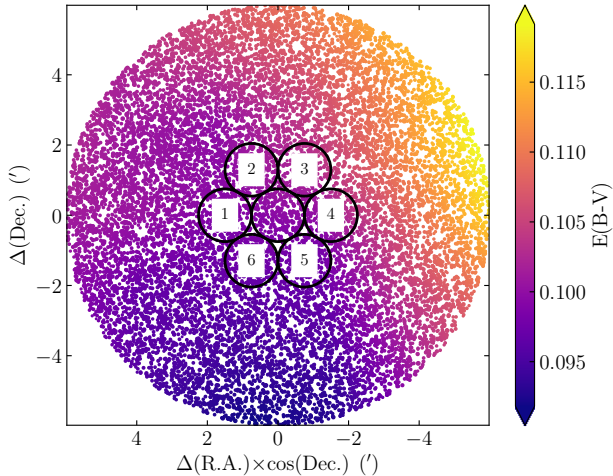


Figure 1. Schematic chart centered on STEP-0029. The size of the symbols is proportional to the g brightness, while their **color excesses** are coded according to the color bar. The radius of the superimposed circles is 3 times that adopted as the cluster’s radius (Gatto et al. 2020). Six labeled reference star fields distributed around the star cluster circle are also drawn.

radial velocities, and/or chemical abundances of individual stars can help with disentangling between field and star cluster members. Unfortunately, in the case of our star cluster sample, *Gaia* DR2 proper motions (Gaia Collaboration et al. 2016, 2018) are unreliable at the main sequence turnoff level ($g_0 \gtrsim 22.0$ mag). When such a piece of information is not available, photometry of reference star fields are usually employed. These reference star fields are thought to be placed far from the star cluster field, but not too far from it as to become unsuitable as representative of the star field projected along the line-of-sight (LOS) of the star cluster. Frequently, it is assumed that the stellar density and the distribution of luminosities and effective temperatures of stars in these reference star fields are similar to those of field stars located along the LOS of the star cluster. However, even though the star cluster is not projected onto a crowded star field or is not affected by differential reddening, it is highly possible to find differences between the astrophysical properties of the reference star fields and the star cluster field. Bearing in mind the above considerations, we decided to clean the star field contamination in the star cluster CMDs by using, at a time, the 6 different devised reference star field areas introduced in Section 2.

The decontamination of a star cluster CMD comprises three main steps, namely: i) to properly deal with each of the 6 reference star fields by considering the observed distribution of their stars in luminosity and effective temperature; ii) to reliably subtract the reference star

fields from the star cluster CMD (one reference field at a time) and, iii) to assign membership probabilities to stars that remained unsubtracted in the resulting cleaned star cluster CMDs. Stars with relatively high membership probabilities can likely be cluster members, if they are placed along the expected star cluster CMD sequences. However, in general, they represent overdensities along the LOS of the composite stellar field population. We refer the readers to Piatti & Bica (2012), who devised the above procedure, which was satisfactorily applied in cleaning CMDs of star clusters projected toward crowded star fields (e.g., Piatti 2017a,b,c, and references therein) and affected by differential reddening (e.g., Piatti 2018a; Piatti et al. 2018a, and references therein).

We used a star cluster field (a circle centered on the cluster with a radius 3 times that of the cluster (see Table B1 in Gatto et al. 2020) to subtract a number of stars equal to that in a reference star field. We repeated the star subtraction for the 6 devised reference star fields (see Fig. 1), separately, one at a time. Note that if we subtracted less or more stars than those in the reference star field, we could conclude on the existence of an unreal stellar excess or on a less populous aggregate, respectively. Moreover, spurious overdensities could even result if the cleaning procedure did choose the stars to subtract following a particular arbitrary spatial pattern (e.g., from North to South). If there were any intrinsic spatial gradient of field stars in the cluster area, the cleaning procedure would eliminate it. The procedure finds field stars in the star cluster CMD (with similar magnitudes and colors as those in the reference star field CMD) where they actually are located, i.e., it subtracts more field stars where they are more numerous.

The distribution of magnitudes and colors of the subtracted stars from the star cluster field needs in addition to resemble that of the reference star field. The method consists in defining boxes centered on the magnitude and color of each star of the reference star field CMD, then to superimpose them on the star cluster CMD, and finally to choose one star per box to subtract. With the aim of avoiding stochastic effects caused by very few field stars distributed in less populated CMD regions, appropriate ranges of magnitudes and colors around the CMD positions of field stars are advisable to be used. Thus, it is highly probable to find a star in the star cluster CMD with a magnitude and a color within those box boundaries. In the case that more than one star is located inside that delimited CMD region, the closest one to the center of that (magnitude, color) box is subtracted. In the present work, we used boxes of $(\Delta g_0, \Delta(g - i)_0)$

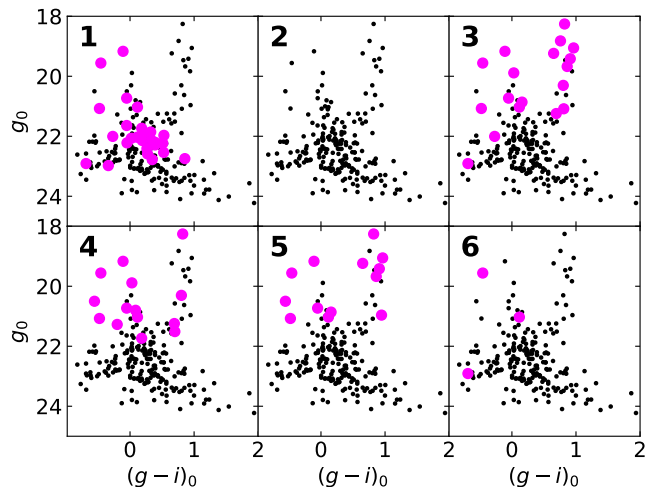


Figure 2. Color-magnitude diagram of STEP-0029. Black points represent all the measured stars in SMASH DR2 data sets located within a circle with a radius equal to 3 times the cluster radius. Large magenta points represent the stars that remained unsubtracted after the CMD cleaning procedure. The reference star field used to decontaminate the star cluster CMD is indicated at the top-left margin (see also Fig. 1).

$= (2.0 \text{ mag}, 1.0 \text{ mag})$ centered on the $(g_0, (g-i)_0)$ values of each reference field star.

In practice, for each reference field star, we first randomly selected the position of a subregion inside the star cluster field where to subtract a star. These subregions were devised as annular segments of 90° wide and of constant area. Their external radii are chosen randomly, while the internal ones are calculated so that the areas of the annular sectors are constant. Here we adopted an area for the subregions equal to πr_{cls}^2 , where r_{cls} is the star cluster radius. We then looked for a star with $(g_0, (g-i)_0)$ values within a box defined as described above. If no star is found in that annular sector, we randomly selected another one and repeated the search, allowing the procedure to iterate up to 1000 times. If no star in the star cluster field with a magnitude and a color similar to $(g_0, (g-i)_0)$ is found after 1000 iterations, we do not subtract any star for that $(g_0, (g-i)_0)$ values. The same procedure was applied for all the stars in the reference star field. The photometric errors of the stars in the star cluster field were also taken into account while searching for a star to be subtracted from the star cluster CMD. With that purpose, we iterated up to 1000 times the search within each defined box, allowing the stars in the star cluster CMD to vary their magnitudes and colors within an interval of $\pm 1\sigma$, where σ represents the errors in their magnitude and color, respectively.

Figure 2 illustrates the different results of the decontamination of field stars when the different 6 reference star fields (see Fig. 1) are used, **separately**. As can be

seen, the different resulting cleaned star cluster CMDs (magenta points) show distinct groups of stars, depending on the reference star field used, which suggests that differences in the astrophysical properties of the composite star field population do exist. If all the reference star fields showed a uniform distribution of stars in magnitude and color, all the resulting cleaned CMDs should look similar. The spatial distribution of the stars that remained unsubtracted is shown in Fig. 3. From Figs. 2 and 3 is readily visible that the stars that have survived the cleaning procedure are not spatially distributed inside the cluster radius (black circle), nor they unquestionably follow the expected sequences in the star cluster CMD either. This means that those stars could rather represent fluctuations in the stellar density along the LOS of the composite stellar field population.

We finally assigned a membership probability to each star that remained unsubtracted after the decontamination of the star cluster CMD. Because the stars in the cleaned CMDs vary with respect to the reference star field employed (see the distribution of magenta points in Figs. 2 and 3), we defined the probability P (%) = $100 \times N/6$, where N represent the number of time a star was not subtracted during the six different CMD cleaning executions. With that information on hand, we built Fig. 4, which shows the spatial distribution and the CMD of all the measured stars located in the field of STEP-0029. Stars with different P values were **plotted** with different colors. We applied the above cleaning procedure to the remaining 16 star cluster candidates discovered by Gatto et al. (2020) with ages $\gtrsim 4$ Gyr, for which SMASH DR2 photometry is available. The resulting SMASH cleaned star cluster CMDs and spatial distribution of the measured stars are shown in Figs. 5 to 7 of the Appendix, while those from STEP/YMCA data sets are depicted in Figs. 8 to 10 of the Appendix.

4. DISCUSSION AND CONCLUSIONS

By examining the spatial distributions of stars with assigned P values (color-coded symbols in Figs. 4, 5-10), none of the analyzed fields show groups of stars with $P > 50\%$ concentrated inside the star cluster radius. This means that the spatial overdensities discovered by Gatto et al. (2020) do not highlight themselves in terms of stellar brightness and color distributions from those of the surrounding field neither in the STEP/YMCA nor SMASH data sets, when the field star decontamination procedure described in Sect. 3 is applied. They could rather reveal small stellar density fluctuations in the studied LMC regions. Isolated stars spread throughout the cleaned areas spanning a wide range of P values are seen in all the studied fields. We also detect

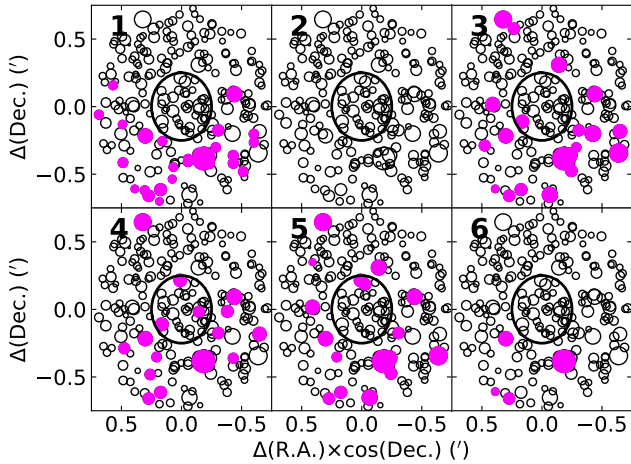


Figure 3. Chart of the stars in the field of STEP-0029. The size of the symbols is proportional to the g brightness of the star. Open black circles represent all the measured stars in SMASH DR2 data sets located within a circle with a radius equal to 3 times the cluster radius. Filled magenta circles represent the stars that remained unsubtracted after the CMD cleaning procedure. The reference star field used to decontaminate the star cluster CMD is indicated at the top-left margin (see also Fig. 1). The large centered circle represents that of the star cluster radius.

some local concentrations of stars that distinguish from the surrounding field in the SMASH data, for example, toward the southern outskirts of STEP-0012, YMCA-0021, and YMCA-0023. Their positions in the cleaned CMDs, however, do not provide hints for any star cluster sequence.

Because of the LMC distance (49.9 kpc; de Grijs et al. 2014), stars projected along a particular LOS could produce CMDs with features similar to those seen in star cluster CMDs. For example, from the SMASH cleaned CMD of YMCA-0002 (Fig. 6), we could conclude on the existence of a star cluster with some few red clump and main sequence turnoff stars, whereas the spatial distribution of stars with $P > 70\%$ does not support such a possibility. The SMASH cleaned CMD of YMCA-0007 shows a populous red clump of stars with $P \sim 50\%$ that belong to the field, as judged by their spatial distribution. In summary, Figs. 4, 5-10 most likely reveal the composite stellar population of the studied LMC regions and their local fluctuations.

Piatti (2018b) arrived to a similar conclusion on the new identified star clusters by Bitsakis et al. (2017), who found that the population of LMC star clusters located at deprojected distances $< 4^\circ$ was nearly double the known size of the system. Piatti (2018b) based his findings on the remarkable large number of objects with assigned ages older than 2.5 Gyr, which contrasts with

the existence of the LMC star cluster age gap; the fact that the assumption of a cluster formation rate similar to that of the LMC star field does not help to reconcile the large amount of star clusters either; and nearly 50% of them come from star cluster search methods known to produce more than 90% of false detections. Bitsakis et al. (2017) identified only $\sim 35\%$ of the previously known cataloged LMC star clusters. The LMC star cluster frequency, i.e., number of star clusters per time unit, is a distribution function that basically does not change if low mass star clusters are not considered. The known LMC star cluster population is statistically complete down to $5 \times 10^3 M_\odot$ and their star cluster frequency does not show clusters in the age-gap, and this is a feature seen all throughout the LMC body (Piatti 2014). The LMC fields analyzed here are located beyond 4° from the LMC center; the number of new detections is not such high; and the recovery fraction of known cataloged LMC star clusters is much higher (see figure 7 in Gatto et al. (2020)). Nevertheless, it is hardly possible that age gap star clusters have been formed only in the outskirts of the LMC. Indeed, the 15 ancient LMC globular clusters are distributed in the halo and in the disk of the galaxy (Piatti et al. 2019).

The different outcomes obtained by Gatto et al. (2020) and in the present work reflect the different performances of the techniques employed for cleaning the CMDs of field star contamination. When comparing the present constructed CMDs (Figs. 4, 5-10) and those of Gatto et al. (2020, see their figure B1) we note that: i) those built from SMASH and STEP/YMCA data contain a similar number of stars and reach in general similar limiting magnitudes per unit area. ii) By comparing the observed and cleaned CMDs built by Gatto et al. (2020), it would seem that the number of field stars subtracted was relatively small. Likewise, the number of stars considered as star cluster members in Gatto et al. (2020)'s CMDs would seem also to be small as to conclude on clear features of a relatively old star cluster. In the present work, we subtracted a larger number of field stars per unit area using the SMASH and STEP/YMCA data sets and no definitive signature of star clusters are observed in the cleaned CMDs. Therefore, we speculate with the possibility that Gatto et al. (2020)'s results and ours are based on a low number statistics. iii) As can be seen, the star distribution along the theoretical isochrones in CMDs built from SMASH and STEP/YMCA data are comparable. Here we stress the issue that for most of the studied objects, those stars would not seem to belong to a physical aggregate, but to the composite LMC field. Indeed, the observed main sequence turnoffs are mostly populated by field stars. iv)

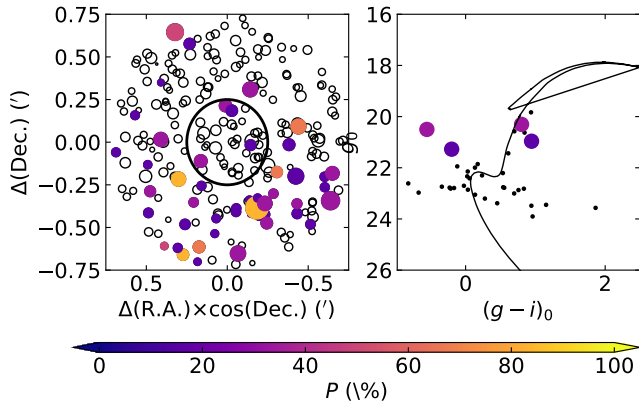


Figure 4. *Left panel:* Chart of the stars in the field of STEP-0029. The size of the symbols is proportional to the g brightness of the star. Open black circles represent all the measured stars in SMASH DR2 data sets located within a circle with a radius equals to 3 times the cluster radius. The large centered circle represents that of the star cluster radius. *Right panel:* Color-magnitude diagram of STEP-0029. Black points represent all the measured stars in SMASH DR2 data sets located within the star cluster radius. The theoretical isochrone plotted by Gatto et al. (2020, see their figure B1) is overplotted for comparison purposes. Filled circles in both panels represent the stars that remained unsubtracted after the CMD cleaning procedure, color-coded according to the assigned membership probabilities (P).

The metallicities of the isochrones used by Gatto et al. (2020) ($Z = 0.004, 0.006$ and 0.008) are much metal-rich than the known metallicity of the only one confirmed LMC age gap cluster ESO 121-SC03 ($Z \approx 0.0015$) (Piatti & Geisler 2013).

Both independent studies point to the need of further deeper observations of these star cluster candidates with the aim of providing a definite assessment on their physical realities. Our analysis shows that STEP/YMCA and SMASH surveys do not have the ability to disentangle the existence of LMC age gap star clusters. The existence of LMC age gap star clusters has been largely treated in the astronomical community, and the general consensus after different focused campaigns for such star clusters and astrophysical results of the star formation history in the LMC has been that ESO 121-SC03 is the only known age gap star cluster.

I thank the referee for the thorough reading of the manuscript and the suggestions to improve it. I warmly thank Vincenzo Ripepi and his team who suggested changes in a previous version of this work.

This research uses services or data provided by the Astro Data Lab at NSF’s National Optical-Infrared Astronomy Research Laboratory. NSF’s OIR Lab is operated by the Association of Universities for Research in Astronomy (AURA), Inc. under a cooperative agreement with the National Science Foundation.

REFERENCES

- Abbott, T. M. C., Abdalla, F. B., Allam, S., et al. 2018, *ApJS*, 239, 18, doi: [10.3847/1538-4365/aae9f0](https://doi.org/10.3847/1538-4365/aae9f0)
- Bekki, K., Couch, W. J., Beasley, M. A., et al. 2004, *ApJL*, 610, L93, doi: [10.1086/423372](https://doi.org/10.1086/423372)
- Bitsakis, T., Bonfimi, P., González-Lópezlira, R. A., et al. 2017, *ApJ*, 845, 56, doi: [10.3847/1538-4357/aa8090](https://doi.org/10.3847/1538-4357/aa8090)
- Choi, Y., Nidever, D. L., Olsen, K., et al. 2018, *ApJ*, 869, 125, doi: [10.3847/1538-4357/aaed1f](https://doi.org/10.3847/1538-4357/aaed1f)
- Da Costa, G. S. 1991, in *IAU Symposium*, Vol. 148, *The Magellanic Clouds*, ed. R. Haynes & D. Milne, 183
- de Grijs, R., Wicker, J. E., & Bono, G. 2014, *AJ*, 147, 122, doi: [10.1088/0004-6256/147/5/122](https://doi.org/10.1088/0004-6256/147/5/122)
- Gaia Collaboration, Prusti, T., de Bruijne, J. H. J., et al. 2016, *A&A*, 595, A1, doi: [10.1051/0004-6361/201629272](https://doi.org/10.1051/0004-6361/201629272)
- Gaia Collaboration, Brown, A. G. A., Vallenari, A., et al. 2018, *A&A*, 616, A1, doi: [10.1051/0004-6361/201833051](https://doi.org/10.1051/0004-6361/201833051)
- Gatto, M., Ripepi, V., Bellazzini, M., et al. 2020, *MNRAS*, 499, 4114, doi: [10.1093/mnras/staa3003](https://doi.org/10.1093/mnras/staa3003)
- Geisler, D., Bica, E., Dottori, H., et al. 1997, *AJ*, 114, 1920, doi: [10.1086/118614](https://doi.org/10.1086/118614)
- Kallivayalil, N., van der Marel, R. P., Besla, G., Anderson, J., & Alcock, C. 2013, *ApJ*, 764, 161, doi: [10.1088/0004-637X/764/2/161](https://doi.org/10.1088/0004-637X/764/2/161)
- Lucchini, S., D’Onghia, E., Fox, A. J., et al. 2020, *Nature*, 585, 203. <https://arxiv.org/abs/2009.04368>
- Maia, F. F. S., Dias, B., Santos, J. F. C., et al. 2019, *MNRAS*, 484, 5702, doi: [10.1093/mnras/stz369](https://doi.org/10.1093/mnras/stz369)
- Mateo, M., Hodge, P., & Schommer, R. A. 1986, *ApJ*, 311, 113, doi: [10.1086/164757](https://doi.org/10.1086/164757)
- Nidever, D. L., Olsen, K., Walker, A. R., et al. 2017, *AJ*, 154, 199, doi: [10.3847/1538-3881/aa8d1c](https://doi.org/10.3847/1538-3881/aa8d1c)
- Nidever, D. L., Olsen, K., Choi, Y., et al. 2021, *AJ*, 161, 74, doi: [10.3847/1538-3881/abceb7](https://doi.org/10.3847/1538-3881/abceb7)
- Olszewski, E. W., Schommer, R. A., Suntzeff, N. B., & Harris, H. C. 1991, *AJ*, 101, 515, doi: [10.1086/115701](https://doi.org/10.1086/115701)
- Piatti, A. E. 2011a, *MNRAS*, 418, L40, doi: [10.1111/j.1745-3933.2011.01139.x](https://doi.org/10.1111/j.1745-3933.2011.01139.x)
- . 2011b, *MNRAS*, 418, L69, doi: [10.1111/j.1745-3933.2011.01145.x](https://doi.org/10.1111/j.1745-3933.2011.01145.x)
- . 2014, *MNRAS*, 437, 1646, doi: [10.1093/mnras/stt1998](https://doi.org/10.1093/mnras/stt1998)

- . 2017a, *ApJL*, 834, L14,
doi: [10.3847/2041-8213/834/2/L14](https://doi.org/10.3847/2041-8213/834/2/L14)
- . 2017b, *MNRAS*, 465, 2748, doi: [10.1093/mnras/stw2987](https://doi.org/10.1093/mnras/stw2987)
- . 2017c, *ApJL*, 846, L10, doi: [10.3847/2041-8213/aa8773](https://doi.org/10.3847/2041-8213/aa8773)
- . 2018a, *MNRAS*, 477, 2164, doi: [10.1093/mnras/sty773](https://doi.org/10.1093/mnras/sty773)
- . 2018b, *MNRAS*, 475, 2553, doi: [10.1093/mnras/stx3344](https://doi.org/10.1093/mnras/stx3344)
- Piatti, A. E., Alfaro, E. J., & Cantat-Gaudin, T. 2019,
MNRAS, 484, L19, doi: [10.1093/mnrasl/sly240](https://doi.org/10.1093/mnrasl/sly240)
- Piatti, A. E., & Bica, E. 2012, *MNRAS*, 425, 3085,
doi: [10.1111/j.1365-2966.2012.21694.x](https://doi.org/10.1111/j.1365-2966.2012.21694.x)
- Piatti, A. E., Cole, A. A., & Emptage, B. 2018a, *MNRAS*,
473, 105, doi: [10.1093/mnras/stx2418](https://doi.org/10.1093/mnras/stx2418)
- Piatti, A. E., & Geisler, D. 2013, *AJ*, 145, 17,
doi: [10.1088/0004-6256/145/1/17](https://doi.org/10.1088/0004-6256/145/1/17)
- Piatti, A. E., Geisler, D., Sarajedini, A., & Gallart, C.
2009, *A&A*, 501, 585, doi: [10.1051/0004-6361/200912223](https://doi.org/10.1051/0004-6361/200912223)
- Piatti, A. E., Hwang, N., Cole, A. A., Angelo, M. S., &
Emptage, B. 2018b, *MNRAS*, 481, 49,
doi: [10.1093/mnras/sty2324](https://doi.org/10.1093/mnras/sty2324)
- Piatti, A. E., & Mackey, A. D. 2018, *MNRAS*, 478, 2164,
doi: [10.1093/mnras/sty1048](https://doi.org/10.1093/mnras/sty1048)
- Piatti, A. E., Sarajedini, A., Geisler, D., Bica, E., & Clariá,
J. J. 2002, *MNRAS*, 329, 556,
doi: [10.1046/j.1365-8711.2002.04994.x](https://doi.org/10.1046/j.1365-8711.2002.04994.x)
- Rich, R. M., Shara, M. M., & Zurek, D. 2001, *AJ*, 122, 842,
doi: [10.1086/321164](https://doi.org/10.1086/321164)
- Ripepi, V., Cignoni, M., Tosi, M., et al. 2014, *MNRAS*,
442, 1897, doi: [10.1093/mnras/stu918](https://doi.org/10.1093/mnras/stu918)
- Sarajedini, A. 1998, *AJ*, 116, 738, doi: [10.1086/300472](https://doi.org/10.1086/300472)
- Schlegel, D. J., Finkbeiner, D. P., & Davis, M. 1998, *ApJ*,
500, 525, doi: [10.1086/305772](https://doi.org/10.1086/305772)

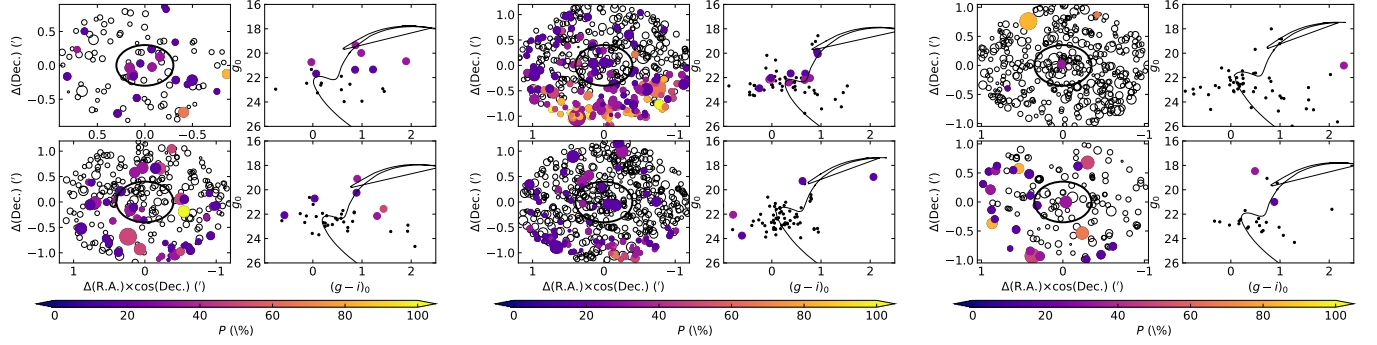


Figure 5. Same as Fig. 4 for STEP-0001, STEP-0005, STEP-0012, STEP-0024, STEP-0035, and YMCA-0001 from top bottom, and from left to right.

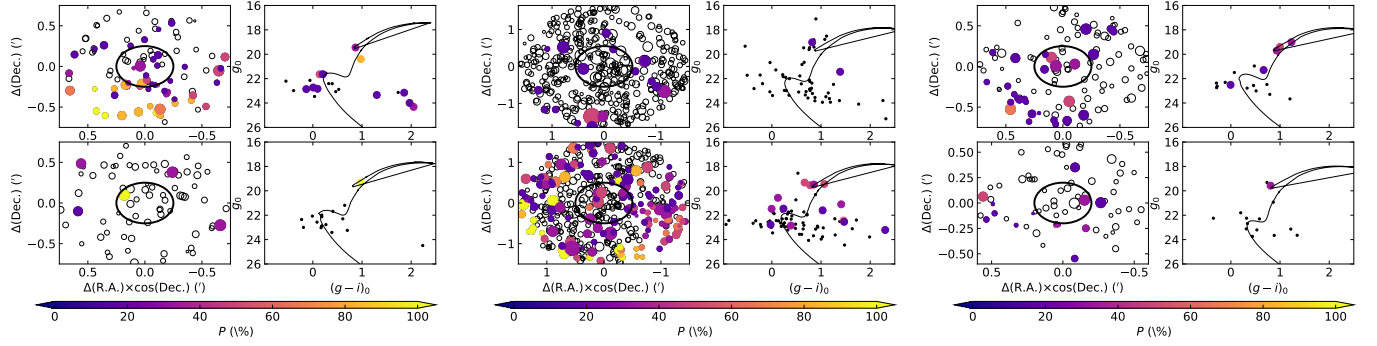


Figure 6. Same as Fig. 4 for YMCA-0002, YMCA-0004, YMCA-0006, YMCA-0007, YMCA-0008, and YMCA-0012 from top bottom, and from left to right.

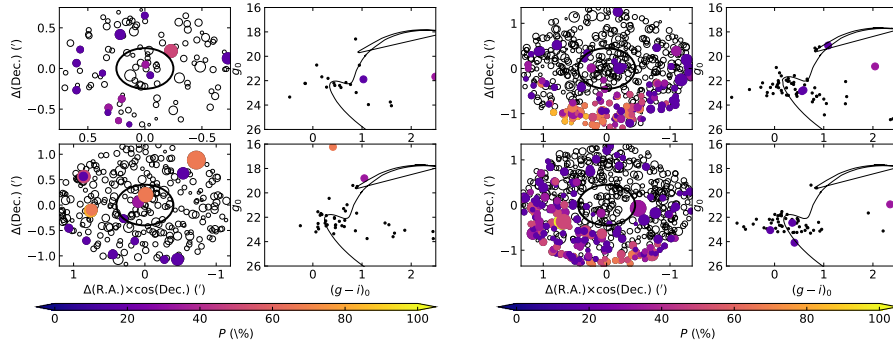


Figure 7. Same as Fig. 4 for YMCA-0013, YMCA-0017, YMCA-0021, and YMCA-0023 from top bottom, and from left to right.

APPENDIX

A. CLEANED STAR CLUSTER CMDS

Figures 5 to 7 show the SMASH cleaned star cluster CMDs and the respective spatial distribution of the star candidates with ages $\gtrsim 4$ Gyr discovered by Gatto et al. (2020). Symbols are as in Fig 4. Figures 8 to 10 are those produced from STEP/YMCA data sets.

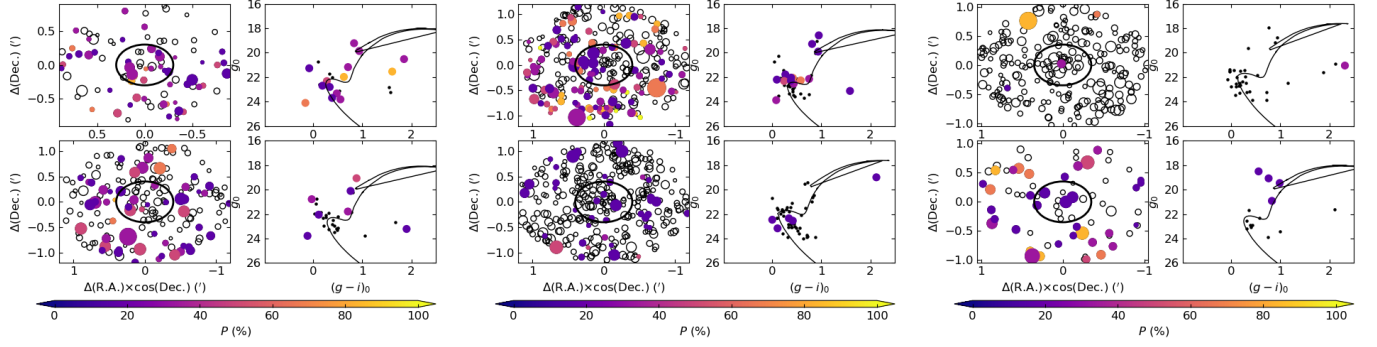


Figure 8. Same as Fig. 4 for STEP-0001, STEP-0005, STEP-0012, STEP-0024, STEP-0035, and YMCA-0001 from top bottom, and from left to right. Data were kindly provided by V. Ripepi.

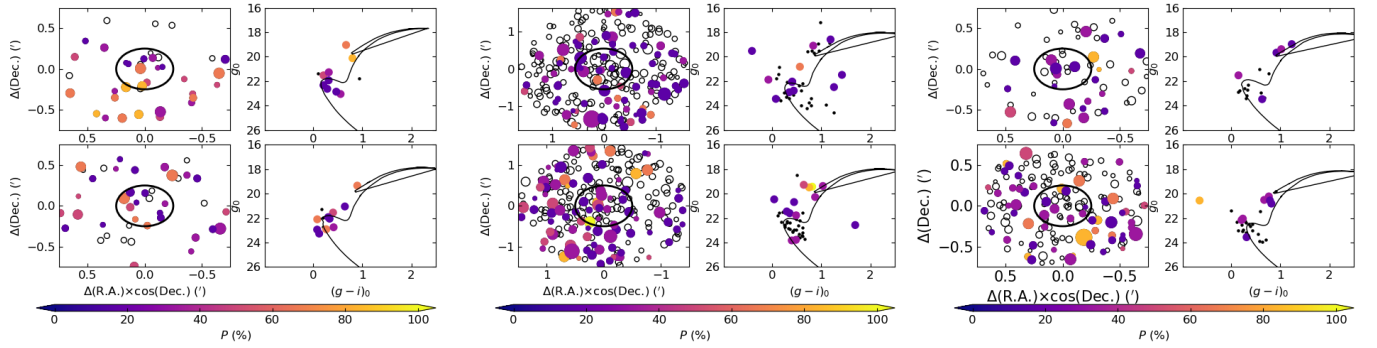


Figure 9. Same as Fig. 4 for YMCA-0002, YMCA-0004, YMCA-0006, YMCA-0007, YMCA-0008, and STEP-0029 from top bottom, and from left to right. Data were kindly provided by V. Ripepi.

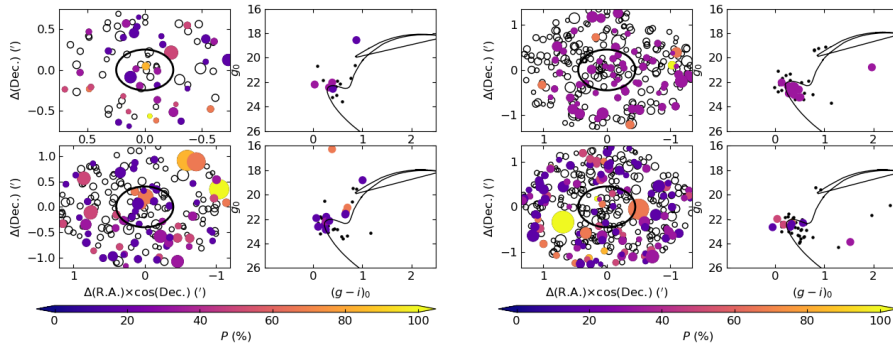


Figure 10. Same as Fig. 4 for YMCA-0013, YMCA-0017, YMCA-0021, and YMCA-0023 from top bottom, and from left to right. Data were kindly provided by V. Ripepi.